

Dynamics of Space-Charge Acceleration of X-Ray Generated Electrons Emitted from a Metal Surface

G.Schiwietz, D.Kühn, A.Föhlisch, K.Holldack, T.Kachel, N.Pontius

*Institut für Methoden und Instrumentierung der Forschung mit Synchrotronstrahlung,
Helmholtz-Zentrum Berlin für Materialien und Energie GmbH, Albert-Einstein-Str. 15,
12489 Berlin, Germany*

Abstract

The so-called vacuum space-charge acceleration of emitted electrons triggered by absorption of soft X-rays (a few 100 eV) under intense near-infrared laser excitation is studied experimentally and theoretically. The influence of high excitation densities on the properties of Auger and photo electrons liberated by a probe X-ray beam is investigated for grazing-incidence photons interacting with an atomically clean Cu (111) surface as a model system. Transient electron spectra have been taken in a pump–probe setup at the BESSY II storage ring using a newly developed compact electrostatic retarding Bessel-box spectrometer. Strong electron-energy shifts have been found and assigned to space-charge acceleration. Model calculations based on experimental input parameters are in good agreement with experimentally obtained energy-gain values indicating ultimate limits of ultrafast X-ray experiments with photo or Auger electrons as a probe.

PACS numbers: *82.80.Pv, 79.60.Bm, 78.47.+p, 71.10.Ay, 32.80.Hd*

Keywords: *Electron Emission; Picosecond-Pump/Probe Experiments;
Short-time Electron Dynamics; Surface Physics; Photo Electrons;
Auger Electrons; Mean-Field Theory*

1. Introduction

Electron spectroscopy provides many tools for the investigation of atoms, molecules, clusters and solids. Excitation by charged particles or electromagnetic radiation enables gaining not only structural information¹, but also detailed insights into electron dynamics, especially if time-resolved measurements are being used.

Modern lasers allow for investigations of ultrafast processes on a fs- or sub-fs-time scale.^{2,3,4} Alternatively, excitation by primary swift heavy ions proceeds also via an electrostatic pulse and may be as fast as 10^{-17} s.⁵ Snapshots of the corresponding electronic time-evolution in the range of 1 to 10 femtoseconds may be extracted from the observation of different ion-induced x-ray- or Auger-decay peak-structures.⁶ Novel excitation sources that allow for time-resolved experiments are free-electron-lasers (FEL) that yield x-ray pulses with a width of only a few fs. These pulses may be used to determine the lattice structure^{7,8} or to investigate short-time dynamics using pump-probe techniques^{9,10}. For pump-probe techniques with FEL or with other strong short pulses of photons as well as for decay-time techniques with fast heavy ions^{6,11}, it is nearly impossible to avoid high degrees of electronic excitation and corresponding non-perturbative effects (this does not hold true for synchrotron radiation based experiments^{12,13} however). Specifically, laser irradiation may yield a huge number of ejected electrons that influence the peak position and structure of all other ejected electrons via electron-electron interaction in the vacuum. Here we study one of the main effects due to strong fs-laser irradiation – space charge acceleration – with special emphasis on maximum energy shifts, delay-time distributions and the influence of the laser-spot shape.

2. Experimental Methods and Spectra

The experimental data and evaluations presented here are based on measurements of the total electron yields and electron spectroscopy of emitted Auger- and photo electrons liberated by the X-ray beam as well as laser-induced electrons. Experiments have been performed at the UE56/1_PGM-1 X-ray beamline^{14,15} at the BESSY II storage ring of the Helmholtz-Zentrum Berlin for X-ray energies between 300 and 1000 eV. We have used our electron-timing (ET) chamber with the newly developed retarding Bessel box (RBB) spectrometer¹⁶ for electron detection. Details of the experiments

involving laser pulses in single-beam as well as pump–probe experiments have been presented in a previous paper.¹⁷

In short, for the excitation we have used a vertically polarized X-ray beam with a broader and nearly collinear near-infrared (NIR) laser beam (wavelength of 800 nm at pulse lengths of about 100 fs). The Cu targets were irradiated by both beams under grazing-incidence conditions (grazing angles were around 20° w.r.t. the target surface). Atomically clean surfaces of Cu (100), Cu (110) and Cu (111) targets (produced by MaTeck company, Germany) have been prepared using cycles of electron-beam heating and Ar-ion sputtering at residual-gas pressures of around 10⁻¹⁰ mbar in the ET chamber. No significant surface coverage has been detected using photo-electron spectroscopy and Auger analysis with incident electrons or X-rays. The crystalline target structure has been verified by observing the angular variation (via target rotation) of the total target current as well as of the Cu-LMM Auger count-rate for an incident electron beam.

Table 1 summarizes typical experimental conditions (energy, energy resolution, depth sensitivity and lateral extensions) regarding the two incident beams (infrared laser and X-rays) as well as of the detected electrons used during the experiments. Further details regarding this table have been published recently.¹⁷ The lateral resolution in the pump-probe experiments is determined locally by the projection of the X-ray beam spot onto the sample surface. The size of the laser induced electron-emission spot, however, determines timing and strength for the space-charge effects. The effective x and y extensions for this spot have been re-adjusted in this work as explained further below.

The electrostatic RBB electron spectrometer was placed in the horizontal plane at 90° with respect to the X-ray beam corresponding to an electron-ejection angle around 70° w.r.t. the target surface. Electron energies between zero and about 1000 eV have been investigated, in order to determine spectra owing to the different processes (photo ionization, Auger decay and purely laser-induced emission) under identical experimental conditions. Additional near-edge X-ray absorption fine structure (NEXAFS) measurements for an Auger line at the Cu-L₃ excitation threshold have also been performed. Absorption spectra with and without laser excitation appear to be identical indicating negligible laser-induced binding energy shifts during the pump–probe experiments.¹⁷ For further detailed target or beam properties and for the methods of time-zero determination and alignment of the different beams, the reader is referred to our previous Cu pump–probe paper.¹⁷

Fig. 1 displays the electron yield per laser pulse Y_{cloud} determined from time-averaged target-current measurements at a laser repetition rate of 6 kHz. The error bars in the y-direction account for electronic noise and target-current fluctuations. The error bars in the x-direction show the estimated absolute uncertainty due to intensity losses within the laser-transfer system of the beamline. Only the first two non-trivial data points of the figure (at 25 and 50 mW) are roughly consistent with the E_{pulse}^3 dependence, expected for 3-photon ionization at low laser-pulse energies E_{pulse} . This indicates that the electron-emission spot might be smaller than the laser spot at small laser powers.^{18, 19} At larger pulse energies we find a nearly linear behavior of Y vs. power, corresponding to a (partial) saturation of the local electron production at the spot center or to space-charge effects within the laser-generated charge cloud.

Fig. 2 displays measured Cu (111) Auger-electron spectra for an X-ray excitation energy of 933 eV (slightly above the Cu-L₃ resonance). The thin red line is an experimental reference curve for pure X-ray excitation and it is completely consistent with previous investigations on Cu targets.²⁰ The corresponding electron escape depth is mainly given by the electron inelastic-mean-free-path (IMFP)²¹ and its values suggests that the top 2 to 5 surface layers of Cu are probed by the electron spectra in this work (see table 1).

The solid blue symbols have been measured in the pump-probe mode (after optimization of the overlap between X-ray and laser beams in space and time) at a mean NIR-laser power of 200 mW for a grazing angle Θ_g of 22° w.r.t. the surface. It is seen that these pump-probe data deviate from the red reference curve by an energy shift towards higher electron energies. The underlying thick solid blue fit curves represent the reference data (cut into three different energy ranges) after a slight intensity adjustment (related to small valence-band modifications) and after a significant shift of the energy scale.¹⁷ The corresponding three energy shifts ΔE are indicated in the plot together with their uncertainties. Similar evaluations have been performed for different emission mechanisms, laser powers, electron energies and pump-probe delays and will be presented in section 4.

3. Model Calculation of Vacuum Space-Charge Acceleration

The physical situation during pump-probe experiments with electron detection is a non-trivial multi-particle problem that is further complicated by the infinite range

of the Coulomb interaction. In order to reduce the complexity of the problem, we restrict ourselves to simplifying boundary conditions:

- 1) We distinguish between a few fast X-ray driven **test electrons** and a much slower laser-induced **electron cloud** that might consist of a huge number of electrons.
- 2) We consider only the case of axial test-electron emission in the direction of the surface normal (z-direction).

Both conditions are roughly in accord with the experimental situation as defined in the previous section. Furthermore, we assume that the time-dependence of the electron cloud may be replaced by its asymptotic motion, related to the experimental energy, angular and time-distributions of laser-induced electrons and their measured total number per laser pulse. Further, we estimate that the mean field leads to a much stronger influence on the test electrons than the stochastic residual electron–electron interaction, the so-called Boersch-effect^{22, 23, 17}, as well as possible Ohmic losses of the moving charges.²⁴

Previously, we have performed mean-field calculations of the electron-energy shift by solving the differential equations (Newton’s equations) for electron motion along the z-direction. For these computations, a cosine-type angular variation of ejected electrons²⁵ and their image charges²⁶ below the metal surface was accounted for.¹⁷ It was shown that condition 1) leads to a simple formula for the energy shift, where the integral over absolute energy- and time-distributions (for sub-ps electron cascades) may exactly be replaced by the measured total electron yield and by a weighted mean energy of the cloud electrons. These previous computations were performed for a uniform circular laser spot on the target, related to an analytical formula for the electric field strength. The theoretical results for the maximum space-charge energy shifts were about 22% lower than the experimental data. It was speculated in that work that the estimated size of the laser spot might be somewhat uncertain and that a Gaussian-like elliptical laser spot might yield other results than a homogeneous circular one (used previously) with an effective radius. Thus, in the following we present results where the analytical electric field is replaced by the more involved numerical integration over 2D charge and image-charge densities as function of the distance between charge cloud and surface. Note that several other model calculations (many of them are Monte-Carlo type multi-electron simulations) exist in the literature^{10, 18, 19, 27, 28, 29, 30, 31}. These are based on different assumptions regarding the angular and

energy distributions of cloud electrons and on the importance of image charges.

Fig. 3 displays our computed delay-time distributions (X-ray minus laser-pulse time) for different shapes of the laser spot on the target. All of them may be characterized as asymmetric cusp-shaped functions. The short-dashed blue curve is computed for a uniform circular spot of fitted size (explained further below). Note that the corresponding radius in the computation is 34% lower than the one estimated previously from the camera picture¹⁷. It is seen that the maximum computed energy shift of about 8.7 eV corresponds to zero delay (for small intrinsic pulse widths). As checked for different cases, the mean width Δt of the calculated time distribution is proportional to the spot size over the electron velocity. Hence, Δt is a mesoscopic quantity.

The thin red curve in Figure 3 shows the data for a uniform elliptical shape involving the same geometrical 1D mean radius (also the same area) as for the radial disk and the experimental aspect ratio of 1:3 for typical grazing angles of the laser beam on the target. The dotted green curve represents the model results for a radial Gaussian distribution with the 1D mean charge radius set equal to the corresponding disk value. At negative times all curves are steeply rising, because test electrons leave the surface before the electron cloud is created. For this condition all the curves are close to each other. The curves differ significantly only at large positive times, when the laser-induced electron cloud is already strongly expanded before the emission of the test electron. Note that the shape of the distribution and the maximum energy shift are strongly influenced by the angular distribution of cloud electrons and by the correct inclusion of the image-charge fields. However, the curves in Fig. 3 are so close to each other that a simple product ansatz for an extrapolation should yield an accurate estimate for an elliptical Gaussian shape of the laser spot (shown as thick long-dashed black line). Exactly this corrected curve is used for comparison with experimental data in the next section.

The results of Figure 3 indicate that the time spectra are nearly independent of the shape of the laser spot when an effective electron emission radius is kept constant. This radius R_{eff} is defined as the geometrical mean of the 1D averages $\langle |x| \rangle$ and $\langle |y| \rangle$ in the x and y direction of the electron-emission spot according to

$$R_{eff} = \sqrt{\langle |x| \rangle \langle |y| \rangle} . \quad (1)$$

For a homogeneous disk, e.g., R_{eff} is exactly half the disk radius R . A consistent modification of our published scaling law¹⁷ for the energy shift $\Delta E_{scaling}$ (valid for high test-

electron energies E_t in comparison to the effective cloud-electron energy E_{cloud}^{eff}) yields for an averaged spot shape

$$\Delta E_{scaling} = b Y_{cloud}/R_{eff} \sqrt{E_{cloud}^{eff}/E_t}, \quad (2)$$

with the adjusted parameter $b = 2.63 \cdot 10^{-9}$ eV m (if ΔE is measured in eV and R in m) and the total electron yield per laser pulse Y_{cloud} (see Figure 1). The effective cloud energy E_{cloud}^{eff} is computed from the broad energy spectrum $\frac{d^2 Y_{cloud}}{d\Omega dE'}$ of the electron cloud by using

$$E_{cloud}^{eff} = \left[\int_0^{E_t} \sqrt{dE'} \frac{d^2 Y_{cloud}}{d\Omega dE'} dE' / \int_0^{E_t} \frac{d^2 Y_{cloud}}{d\Omega dE'} dE' \right]^2. \quad (3)$$

The interpolated experimental results (determined previously from low-energy electron spectra of laser generated electrons) for this parameter are 6.1, 9.3, 10.0, 12.0 eV for laser powers of 75, 125, 150, 200 mW at a 6 kHz repetition rate.¹⁷ Note that these formulas are valid only for pulse widths (laser and x-ray pulse) that are small compared to the typical width of the delay-time distribution, which is roughly given by the ratio of R_{eff} over the mean cloud velocity (about 50 ps may be extracted from Figure 3). For very long x-ray and/or laser pulses the delay curve will be determined by those pulse widths.

4. Results and Discussion

Fig. 4 displays different types of time distributions vs. the X-Ray time-delay. The upper plot shows model results only. The blue dashed curve shows the results for full numerical calculations of the electron-energy shift extrapolated towards an elliptical Gaussian laser-induced spot on the sample. This is exactly the ‘corrected’ curve in Fig. 3. The solid thick olive curve in Fig. 4 is computed from the dashed curve by applying a Fourier transform low-pass filter. The chosen filter parameter corresponds to a convolution with a typical X-ray pulse (20.5 ps FWHM³² for the measured value of 0.43 mA in the laser-synchronized bunch) for the low- α mode of the storage ring. The use of a simple convolution in time for simulating the influence of time structures on the mean-energy shift is suggested by the linear Y_{cloud} dependence in Eq. 2.

The lower plot shows ratios of the electron intensity with and without laser excitation. The symbols with error bars (all-over uncertainty) show experimental data taken for the same laser and X-ray parameters as used for the electron spectra in Fig. 2. However, for the lower plot in Fig.4 the detected electron energy was set to the

fixed value of $E_0=940$ eV and the delay time was scanned. This means we have selected the high-energy wing of the Cu L_3 -VV Auger structure and any positive energy shift in the range of 0 to 30 eV leads to enhanced electron yields. The two curves in the lower plot correspond to the same parameters as in the experiment and result directly from the two curves in the upper plot. The plotted energy shifts ΔE have been transformed into simulated intensity ratios R by using $R=Y(E_0-0.75 \Delta E(\Delta t))/Y(E_0)$, where $Y(E)$ is the undisturbed energy spectrum in Fig. 2 (the thin red curve). It is seen that there is a nearly perfect agreement between theoretical and experimental data, except for the scaling factor 0.75 that simplifies the comparison of the experimental and theoretical shapes. As discussed in relation to Fig. 1, the electron-emission spot might be smaller than the size of the laser spot, consistent with the findings of other authors^{18, 19}. Fitting of this spot size for a fixed aspect ratio of 3 has resulted in 0.264×0.792 mm (about 34% smaller than the estimated laser-spot size), considered for all model results given in this paper.

Fig. 5 displays experimental and theoretical electron-energy shifts for different undisturbed electron energies and NIR-laser powers at fixed laser repetition frequency of 6 kHz for grazing-incidence angles. The measured energy enhancements are extracted from the energy difference of Auger-electron or photo-electron peaks with and without the NIR pump-laser beam, after re-adjustment of the laser focus and time-delay setting. The plotted experimental data points show our previously published results¹⁷, except for the 200-mW values that have been re-evaluated (see Fig. 2) and extended. The shifts are monotonically decreasing with increasing kinetic electron energy and with reduced laser power.

The four solid and dashed curves in Fig. 5 correspond to absolute theoretical results for the different laser powers. These results have been calculated for an elliptical laser spot at $\Delta t=0$ and corrected for the influence of a non-uniform laser density (Gaussian) as well as for the effect of the convolution with the low- α pulse width (see Fig. 4). Test calculations for different energies yield a nearly energy-independent correction factor of ~ 0.86 . There is good agreement of these theoretical ab-initio accelerations with our experimental data (without any intensity fit). The 200-mW values might be an exception from this finding, as the model results seem to exceed the experimental data by about 14% ($\sim 1.5 \sigma$) and a 25% deviation was also found in Fig. 4. Specifically for this case, the cloud-electron density might be so high that there is a

redistribution of electrons within the cloud (Coulomb explosion), turning the initial cosine angular distribution towards isotropic.¹⁷

Replacing the image charges by rigid surface charges (expected for insulators without electronic polarizability) in our model reduces the computed energy shift by about a factor of 2. Neglecting all the compensating positive charges due to ionization or polarization (as often used in simplified model calculations) enhances the energy shift by about a factor of 5. Thus, the good agreement between model and experimental data points to the importance of adiabatic image charges.

5. Conclusions and Outlook

We have performed our experiments with well-defined metallic targets. Further, we have also characterized the boundary conditions of space-charge acceleration by measuring the energy distribution of laser-induced electrons and their total number per laser pulse. The pump–probe measurements have been performed with laser-repetition rates of 6 kHz and reference spectra without laser excitation have been taken simultaneously at an X-ray-repetition rate of a few hundred MHz, given by the bunch separation in the electron-storage ring. We have found vacuum space-charge accelerations corresponding to energy gains of nearly 10 eV for the X-ray driven electron emission during laser irradiation.

In this paper, we have performed more detailed ab-initio model calculations of the vacuum space-charge acceleration based on our experimental data of the laser-induced electron cloud that defines the mean acceleration field. Special emphasis was devoted to the influence of the shape of the laser spot and to the delay-time dependence of energy shifts. Specifically, it was found that the different focal shapes (Gaussian vs. uniform elliptical and circular disk) lead to similar results when the mean 1D radius R_{eff} is kept constant. Comparison between experiment and theory indicates that the variation of the energy shift of Auger and photo electrons for different parameters (test-electron energy, laser power, delay time) is well understood. The good agreement with our computed energy shifts even on an absolute scale (after determining the effective emission-spot size and after convolution with the X-ray pulse width), shows the predictive power of the model. This type of mean-field model may be applied to FEL radiation and other types of space-charge energy shifts as well. It is emphasized that the long-ranged nature of the electrostatic acceleration process leads to a cusp shaped delay curve, typically on a ps time-scale. Experimentally, a dominant ps-cusp

of the energy shift is an indication that a possible underlying femtosecond dynamics might be overshadowed by space-charge effects.

Acknowledgements

We are indebted to the BESSY-II operation team, to R.Mitzner for his help at the pump laser and to M.Beye for helpful comments and experimental contributions. The setup was mainly financed via the Helmholtz strategy fund "Ionenspuren in Festkörpern" (2000-2005). Last but not least, we should mention the help of the BESSY mechanics workshop and of T.Blume regarding the optimization of the setup.

Tables, Figures and Captions

Table 1: Typical parameters for incident photons and escaping electrons used in this work

	Energy E_X , E_{IR} , or E_e	Reso-lu- tion $\Delta E/E$	Attenuation / Escape Depth d	Spot Size (horizontal) x_{eff}	Spot Size (vertical) y_{eff}
X-ray	315 – 1000 eV	< 0.1%	15 – 250 nm	270 μm	60 μm
IR-laser	1.55 eV	< 0.5%	3 – 5 nm	792 μm	264 μm
Electrons	20 – 1000 eV	3%	0.5 – 1.7 nm	–	–

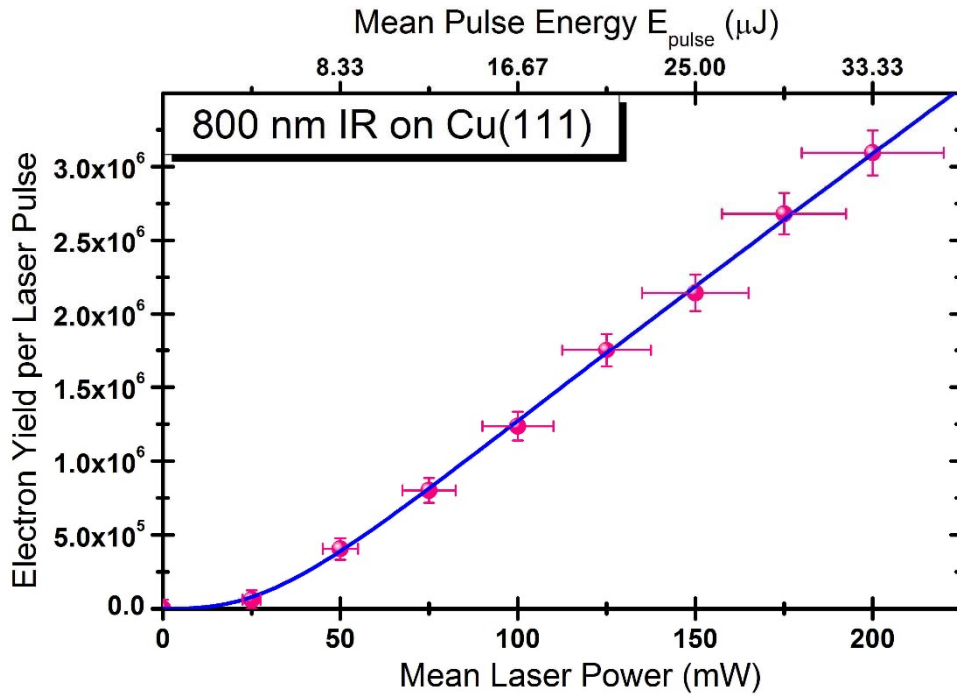


Fig. 1: (color online) Total electron yield as a function of the mean NIR-laser power, respectively the mean energy per laser pulse E_{pulse} , taken at a grazing angle θ_g of 25° with respect to the surface. The solid blue curve serves to guide the eye and starts with the expected asymptotic perturbative dependence ($\sim E_{\text{pulse}}^3$) at low pulse energies.

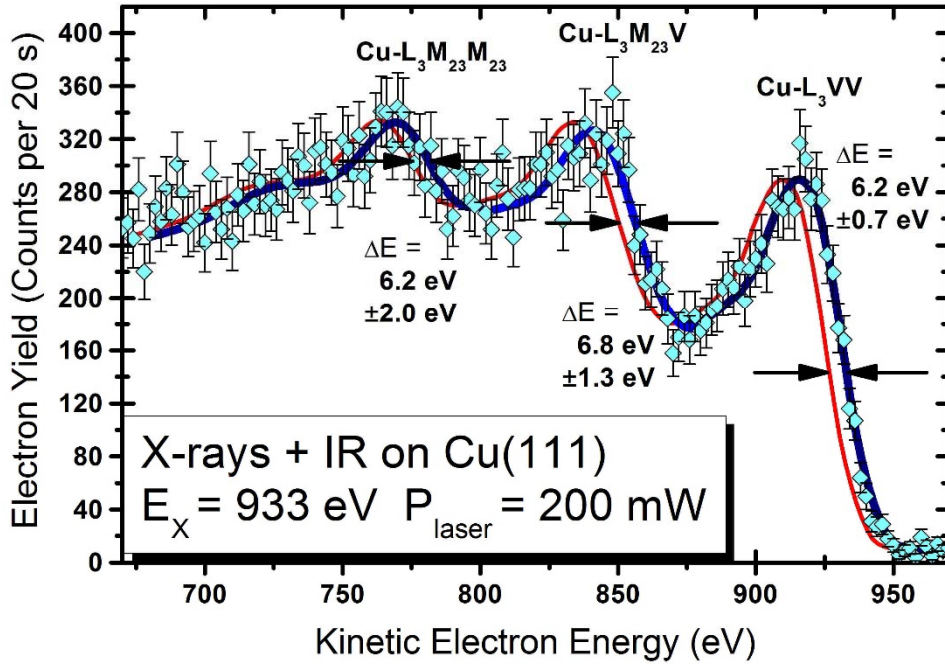


Fig. 2: (color online) Electron-energy spectra for the L_3 Auger decay in Cu (111). The three visible Auger maxima correspond to L_3 -Auger transitions involving different combinations of the initial M_{23} shell and the valence band (V). For vertical polarization, a background due to valence-band photo ionization is about 10% below the $\text{Cu-L}_3\text{VV}$ line. The solid symbols have been measured in the pump-probe mode in the BESSY low-alpha mode at an optimized delay and the thin red curve shows experimental reference data taken simultaneously without laser excitation (the thick solid blue fit curves are explained in the text). The mean NIR-laser power is 200 mW (33 μJ per pulse) in the pump-probe case and all data have been taken for vertically polarized X-rays at a primary photon energy of about 933 eV (at the Cu-L_3 resonance maximum) and a grazing angle θ_g of 22° with respect to the surface

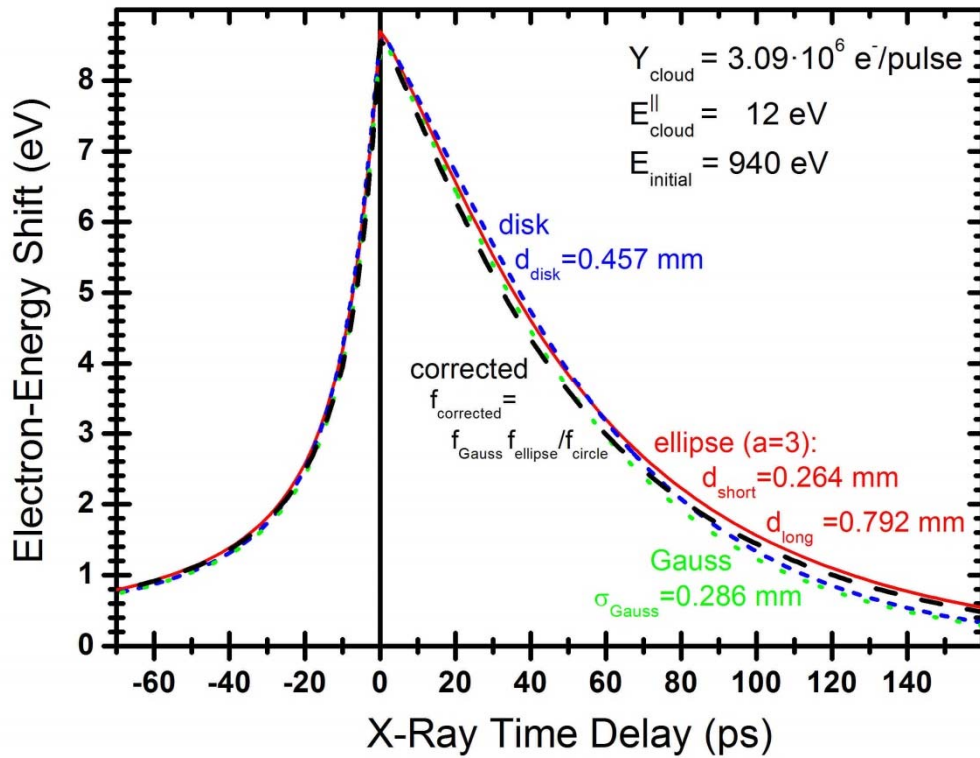


Fig. 3: (color online) Computed delay-time distributions for three different shapes of the electron-emission spot on the target (short-dashed blue curve: circular disk, thin red curve: elliptical shape, dotted green curve: Gaussian radial distribution) with identical effective radii (see text). The thick long-dashed black curve corresponds to an extrapolation that describes an elliptical Gaussian shape of the laser spot.

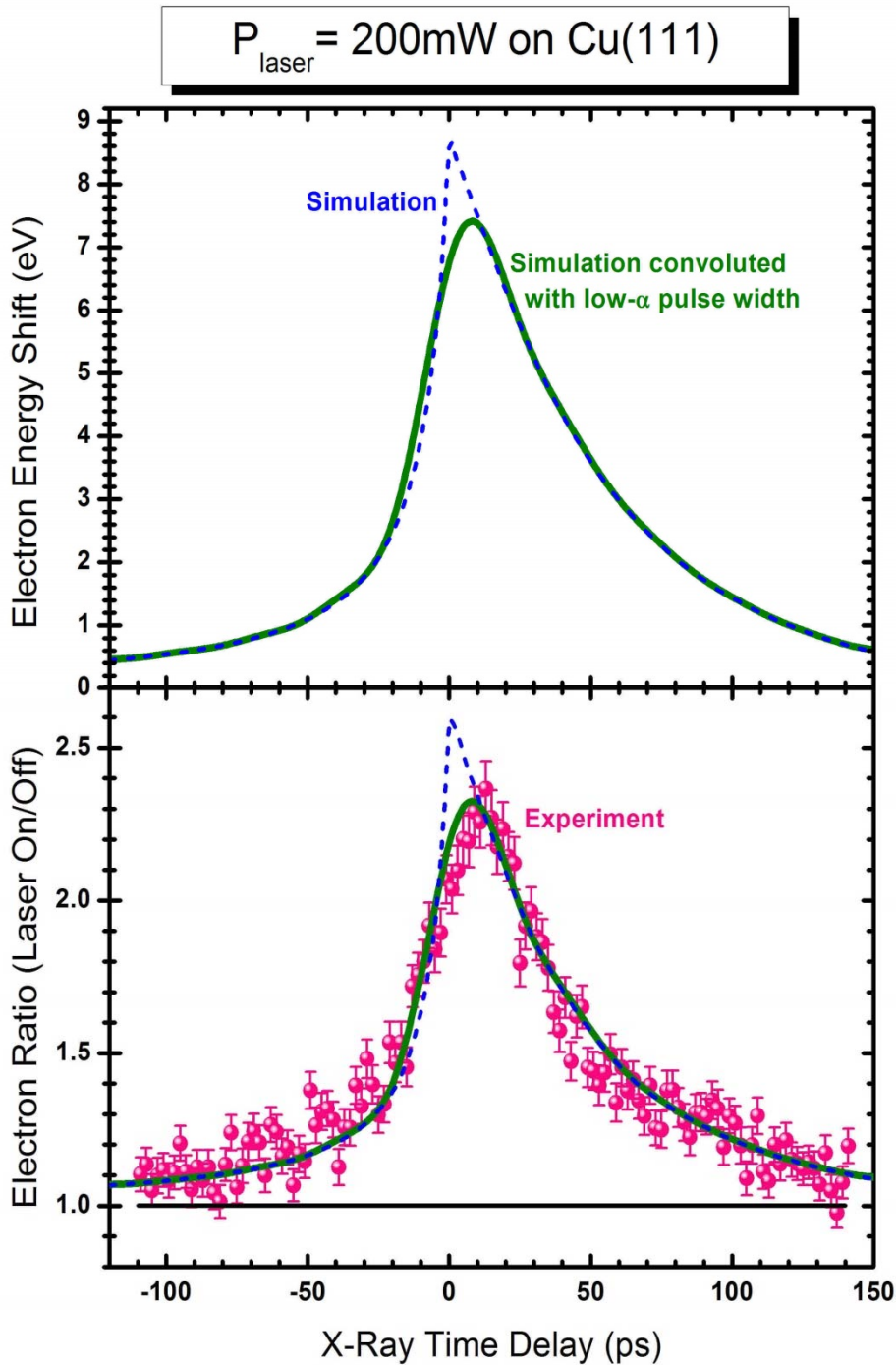


Fig. 4: (color online) Time distributions vs. X-Ray time-delay w.r.t the laser pulse. Upper plot: full simulation of the electron-energy shift (blue dashed curve) and the same results convoluted with the low- α X-Ray pulse length (thick olive curve). Lower plot: the results plotted above transformed into a simulated intensity ratio (after a 25% reduction of the shift, for better comparison). The symbols with statistical error bars show experimental results taken under exactly the same conditions (see Fig. 2).

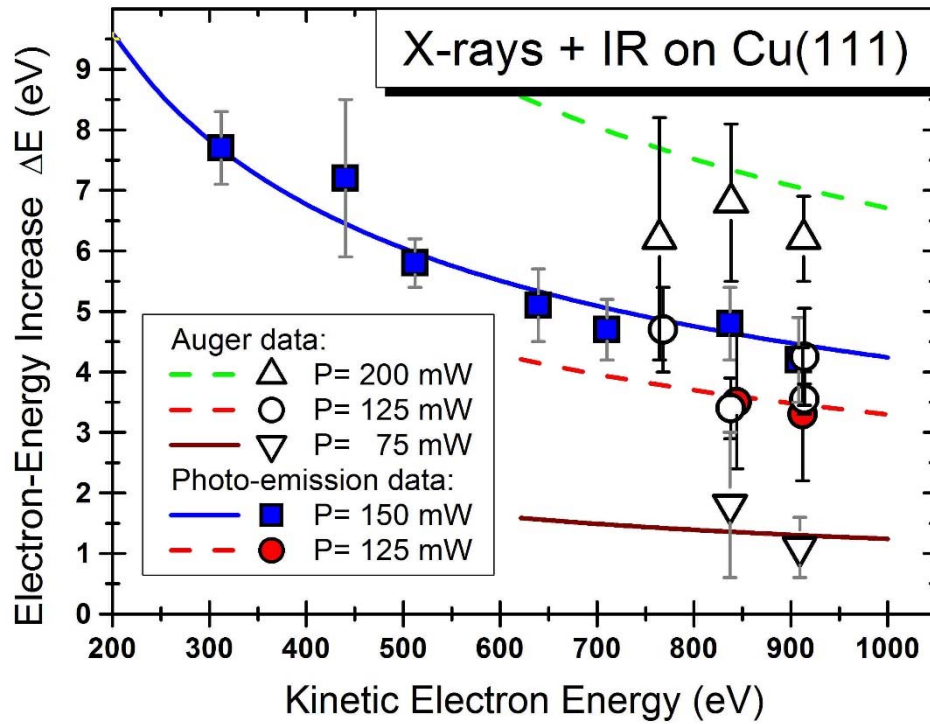


Fig. 5: (color online) Electron-energy enhancements extracted from the energy difference of electron peaks with and without the NIR pump-laser beam. Results have been obtained for different photon energies and NIR-laser powers: at mean values of 200 mW (open up triangles), 150 mW (blue squares), 125 mW (red and open circles), and 75 mW (open down triangles). Closed (colored) symbols indicate values that have been determined from photo-ionization peaks. All open symbols are related to shifts of Auger-electron peaks. The curves correspond to the absolute theoretical results for the 4 different laser powers as described in the text.

References

- ¹ NIST Standard Ref. Database **100** for the *Simulation of Electron Spectra for Surface Analysis* (SESSA 1.1); see also W. Smekal, W. S. M. Werner, and C. J. Powell, *Surf. Interface Anal.* **37** (2005) 1059.
- ² T. Hertel, E. Knoesel, M. Wolf, and G. Ertl, "*Ultrafast Electron Dynamics at Cu(111): Response of an Electron Gas to Optical Excitation*", *Phys. Rev. Lett.* **76** (1996) 535.
- ³ A.T. Yeh, C.V. Shank, J.K. McCusker, "*Ultrafast Electron Localization Dynamics Following Photo-Induced Charge Transfer*", *Science* **289/5481** (2000) 935-938
- ⁴ F. Krausz, and M. Ivanov, "*Attosecond Physics*", *Rev. Mod. Phys.* **81**, (2009) 163-234.
- ⁵ P.L. Grande and G. Schiwietz, "*Ionization and energy loss beyond perturbation theory*", in *Advances in Quantum Chemistry*, Vol. **45** Part 1 (book article ed. by J. Sabin, 2004, Elsevier Inc.) 7-46.
- ⁶ G. Schiwietz, M. Roth, K. Czerski, F. Staufenbiel, and P.L. Grande, "*Femtosecond Dynamics: Snapshots of the Early Ion-Track Evolution*", *Nucl. Instr. Meth.* **B226** (2004) 683-704; and references therein; G. Schiwietz, K. Czerski, M. Roth, P. L. Grande, V. Koteski, and F. Staufenbiel, "*Evidence for an Ultrafast Breakdown of the BeO Band Structure Due to Swift Argon and Xenon Ions*", *Phys. Rev. Lett.* **105** (2010) 187603.
- ⁷ H.N. Chapman et al., "*Femtosecond diffractive imaging with a soft-X-ray free-electron laser*", *Nature Physics* **2** (2006) 839-843.
- ⁸ M.E. Couprie, "*New generation of light sources: Present and future*", *Journal of Electron Spectroscopy and Related Phenomena* **196** (2014) 3-13.
- ⁹ U. Fröhling et al., "*Single-shot terahertz-field-driven X-ray streak camera* ", *Nature Photonics* **3** (2009) 523-528.
- ¹⁰ S. Hellmann, K. Rossnagel, M. Marczyński-Bühlow, and L. Kipp, "*Vacuum space-charge effects in solid-state photoemission*", *Phys. Rev.* **B79**, (2009) 035402; S Hellmann, C. Sohrt, M. Beye, T. Rohwer, F. Sorgenfrei, M. Marczyński-Bühlow, M. Kalläne, H. Redlin, F. Hennies, M. Bauer, A. Föhlisch, L. Kipp, W. Wurth and K. Rossnagel, "*Time-resolved x-ray photoelectron spectroscopy at FLASH*", *New Journal of Physics* **14** (2012) 013062.

-
- ¹¹ G. Schiwietz, P.L. Grande, B. Skogvall, J.P. Biersack, R. Köhrbrück, K. Sommer, A. Schmoltdt, P. Goppelt, I. Kádár, S. Ricz, U. Stettner, "*Influence of Nuclear Track Potentials in Insulators on the Emission of Target Auger Electrons*", Phys. Rev. Lett. **69** (1992) 628-631; G. Schiwietz, G. Xiao; "*Electron Ejection from Solids Induced by Fast Highly-Charged Ions*", Nucl. Instr. Meth. **B107** (1996) 113-127; G. Schiwietz, G. Xiao, E. Luderer, and P.L. Grande, "*Auger Electrons from Ion Tracks*", Nucl. Instr. Meth. **B164-165** (2000) 353-364.
- ¹² O. Björneholm, A. Nilsson, A. Sandell, B. Hernnäs, and N. Mårtensson, "*Determination of time scales for charge-transfer screening in physisorbed molecules*", Phys. Rev. Lett. **68** (1992) 1892.
- ¹³ A. Föhlisch, P. Feulner, F. Hennies, A. Fink, D. Menzel, D. Sanchez-Portal, P.M. Echenique, and W. Wurth, "*Direct observation of electron dynamics in the attosecond domain*", Nature **436** (2005) 373-376.
- ¹⁴ K.Holldack, J.Bahrtdt, A.Balzer, U.Bovensiepen, M.Brzhezinskaya, A.Erko, A.Eschenlohr, R.Follath, A.Firsov, W.Frentrup, L.Le Guyader, T.Kachel, P.Kuske, R.Mitzner, R.Müller, N.Pontius, T.Quast, I.Radu, J.-S.Schmidt, C.Schüßler-Langeheine, M.Sperling, C.Stamm, C.Trabant, and A.Föhlisch, "*FemtoSpeX: a versatile optical pump–soft X-ray probe facility with 100 fs X-ray pulses of variable polarization*", J. Synchrotron Rad. **21** (2014) 1090-1104.
- ¹⁵ N.Pontius, K.Holldack, C.Schüßler-Langeheine, T.Kachel, R.Mitzner, "*The FemtoSpeX facility at BESSY II*", Journal of large-scale research facilities **2** (2016) A46.
- ¹⁶ G. Schiwietz, M. Beye, D. Kühn, and G. Xiao, "*The retarding Bessel Box—An electron spectrometer designed for pump/probe experiments*", Journal of Electron Spectroscopy and Related Phenomena **203** (2015) 51-59
- ¹⁷ G.Schiwietz, D.Kühn, A.Föhlisch, K.Holldack, T.Kachel, N.Pontius, "*Laser-Pump X-Ray-Probe Experiments with Electrons ejected from a Cu(111) target: Space-Charge Acceleration*", Journal of Synchrotron Radiation **23/5** (2016) 1158-1170; see references therein. Note that the radius R_0 in eq. 5 of that paper has to be replaced by the corresponding diameter $2R_0$.
- ¹⁸ S. Passlack, S. Mathias, O. Andreyev, D. Mittnacht, M. Aeschlimann and M. Bauer, "*Space charge effects in photoemission with a low repetition, high intensity femto-second laser source*", Journal of Applied Physics **100**, 024912 (2006).

-
- ¹⁹ D. Leuenberger , H. Yanagisawa , S. Roth , J. Osterwalder , and M. Hengsberger, "*Disentanglement of electron dynamics and space-charge effects in time-resolved photoemission from h-BN/Ni(111)* ", Phys. Rev. B **84**, 125107 (2011).
- ²⁰ R. Courths and S. Hüfner, "*Photoemission experiments on Copper*", Phys. Rep. **112** (1984) 55-171
- ²¹ NIST Standard Ref. Database **71**, NIST Electron Inelastic-mean-free-path database version 1.1; by C. J. Powell and A. Jablonski (2000)
- ²² H. Boersch, "*Experimentelle Bestimmung der Energieverteilung in thermisch ausgelösten Elektronenstrahlen*", Z. Phys. **139** (1954) 115-146.
- ²³ G.H. Jansen, "*Coulomb interactions in particle beams*", J. Vac. Sci. Technol. **B6** (1988) 1977-1983.
- ²⁴ R. Joynt, Science **284**, 777-779, 1999
- ²⁵ M. Rösler, "*Theory of particle-induced kinetic electron-emission from simple metals*", Appl. Phys. **A61** (1995) 595-607; M. Rösler and W. Brauer, "*Theory of secondary-electron emission I. General theory for nearly-free-electron metals*", Phys. Stat. Sol. **B104/1** (1981) 161-175.
- ²⁶ G. Xiao, G. Schiwietz, P.L. Grande, N. Stolterfoht, A. Schmoltdt, M. Grether, R. Köhrbrück, A. Spieler, U. Stettner, "*Indications of Nuclear-Track-Guided Electrons Induced by Fast Heavy Ions in Insulators*", Phys. Rev. Lett. **79** (1997) 1821-1824.
- ²⁷ X.J.Zhou, B.Wannberg, W.L.Yang, V.Brouet, Z.Sun, J.F.Douglas, D.Dessau, Z.Hussain and Z.-X.Shen, "*Space charge effect and mirror charge effect in photoemission spectroscopy*", J. Electron Spectrosc. Relat. Phenom. **142** (2005) 27-38.
- ²⁸ G. Schönhense, K. Medjanik, C. Tusche, M. de Loos, B. van der Geer, M. Scholz, F. Hieke, N. Gerken, J. Kirschner, W. Wurth, "*Correction of the deterministic part of space-charge interaction in momentum microscopy of charged particles*", Phys. Ultramicroscopy **159/3** (2015) 488-496.
- ²⁹ M. Dell'Angela, T. Anniyev, M. Beye, R. Coffee, A. Föhlisch, J. Gladh, S. Kaya, T. Katayama, O. Krupin, A. Nilsson, D. Nordlund, W. F. Schlotter, J. A. Sellberg, F. Sorgenfrei, J. J. Turner, H. Öström, H. Ogasawara, M. Wolf and W. Wurth, "*Vacuum space charge effects in sub-picosecond soft X-ray photoemission on a molecular adsorbate layer*", Struct. Dyn. **2** (2015) 025101.

-
- ³⁰ A. Verna, G. Greco, V. Lollobrigida, F. Offi and G., Stefani, "*Space-charge effects in high-energy photoemission*", *Journal of Electron Spectroscopy and Related Phenomena* **209** (2016) 14-25 and references therein.
- ³¹ L.-P. Oloff, M. Oura, K. Rossnagel, A. Chainani, M. Matsunami, R. Eguchi, T. Kiss, Y. Nakatani, T. Yamaguchi, J. Miyawaki, M. Taguchi, K. Yamagami, T. Togashi, T. Katayama, K. Ogawa, M. Yabashi and T. Ishikawa, "*Time-resolved HAXPES at SACLA: probe and pump pulse-induced space-charge effects*", *New Journal of Physics* **16** (2014) 123045; L.-P. Oloff, K. Hanff, A. Stange, G. Rohde, F. Diekmann, M. Bauer, and K. Rossnagel, "*Pump laser-induced space-charge effects in HHG-driven time- and angle-resolved photoelectron spectroscopy*", *Journal of Applied Physics* **119/22** (2016).
- ³² R. Müller, T. Birke, F. Falkenstern, H. Glass, P. Kuske, R. Ovsyannikov A. Schällicke, D. Schüler, and K. Holldack, "*BESSY II supports an extensive suite of timing experiments*", *Proceedings of IPAC2016 (Busan, Korea, 2016)* 2840-2843.